journal

J. Am. Ceram. Soc., 97 [7] 2272–2278 (2014)
DOI: 10.1111/jace.12889
© 2014 The American Ceramic Society

Kinetics of Cristobalite Formation in Sintered Silica

Ryan C. Breneman†,* and John W. Halloran**

Department of Material Science and Engineering, University of Michigan, Ann Arbor, MI

The kinetics of the cristobalite transformation are reported for sintered silica glass from 1200°C to 1650°C and plotted as a time–temperature–transformation diagram. The 1200°C–1350°C transformation data were fit to the Johnson–Mehl–Avrami–Kolmogorov expression with an time exponent of 3.0 ± 0.6 and an apparent activation energy of 555 ± 24 kJ/mol for the kinetic constant. The temperature of maximum transformation rate was found to fall between 1500°C and 1600°C. Seeding amorphous silica powder with cristobalite resulted in accelerated transformation kinetics. Silica glass powder containing residual quartz had faster transformation kinetics than fully amorphous powder seeded with cristobalite.

I. Introduction

Amorphous silica is widely used as a high temperature glass, electrical insulator, optical material, and refractory. In many silica applications, it is crucial to control the transformation to cristobalite. Cristobalite formation sets the upper temperature bound for use of fused silica glassware; whereas, in glass ceramics and silica refractories, the formation of cristobalite is a vital part of processing. The devitrification of silica to cristobalite has a long history of study in many contexts. Research on the transformation to cristobalite in bulk glasses was conducted by Ainslie et al[1] in 1962 and by Wagstaff and Richards[2] in 1965. Cristobalite formation in gels was studied by Verduch[3] in 1962 and by Chao and Lu[4] in 2000. The transformation in powdered and sintered silica was studied by Wang and Hon[5] in 1995, Li et al[6] in 2008, and Kazemi et al[7] in 2013. Despite being studied in many contexts and forms across several decades the silica transformation to cristobalite remains less defined and quantified than many silica-derived glass ceramics. Perhaps this arises from the sensitivity of the system to impurities. It was noted by Wagstaff and Richards,[8] and many since,[9–11] that the devitrification of silica is sensitive to moisture in the air and trace impurities. In this study, we have examined the cristobalite transformation in a 99.7% pure, commercial refractory silica powder. As this material is an industrial silica, we expect that the behavior will differ from purer laboratory and electronics grade silica. Indeed, it was found that this material has faster transformation kinetics than any reported pure silica, but slower transformation kinetics than reported for doped glass systems.

We collected data for the degree of crystallization versus annealing time and temperature for sintered silica powder. At temperatures between 1200°C–1350°C, the porosity and surface area did not change during the crystallization anneal. The results could be fit to an expression based on the Johnson–Mehl–Avrami–Kolmogorov model, JMAK, and this was used to construct Time–Temperature–Transformation or TTT diagrams. For this temperature range, the TTT diagram is linear, as it represents the low temperature leg of the full TTT diagram. At higher temperatures there is a maximum crystallization rate, corresponding to the "nose" of the TTT diagram. We were able to explore the transformation rate around the nose with a set of experiments from 1400°C–1650°C, but in this range, the glassy powders sintered and densified concurrently with crystallization, which complicates the analysis.[12,13] The effect of seeding amorphous silica powders with powdered cristobalite was studied by comparison of crystallization kinetics in seeded and unseeded silica powders. The effectiveness of seeding with powder cristobalite was also compared to the effect of residual quartz in incompletely amorphized silica glass powder.

II. Procedure

(1) Materials

Fused silica ceramics were prepared with commercially available industrial silica of 99.7% purity with 5% residual quartz content, (TECO-Sphere-Microdust; CE Minerals, Greeneville, TN). The predominant impurities are 2000 ppm alumina and 250 ppm iron oxide. Calcium, Magnesium, Sodium, and Potassium oxides are present in concentrations of less than 50 ppm each. As determined by dynamic light scattering with a Microtrac X-100, mean particle size by volume is 10.3 μm, the D10 2.5 μm, the D50 6.7 μm, and the D90 22.0 μm. The powder is largely composed of 5–25 μm spheriodized particles with a small volume fraction of irregular, fine particles under 0.5 μm. This silica is spheroidized by a drop furnace process, in which ground quartz powder is dropped through a hot furnace which heats it to melting. This simultaneously transforms the crystalline quartz starting material to amorphous silica while causing particles to adopt a spherical shape. The quartz content is remnant crystallinity due to incomplete amorphization during the process. The crystalline content and phase were verified by X-ray Diffraction.

For the powder comparison study, a fully amorphous silica powder was used (TECO-Sphere-A; CE Minerals, Greeneville, TN). The fully amorphous powder of 99.7% purity (TECO-Sphere-A; CE Minerals) was compared to the material with 5% residual quartz (TECO-Sphere-Microdust; CE Minerals). The fully amorphous powder has a similar size distribution, with the mean particle size by volume is 7.45 μm, the D10 2.2 μm, the D50 4.64 μm, and the D90 16.0 μm. This fully amorphous powder is also spheriodized by a drop furnace process, but it differs in that the starting material is amorphous silica powder rather than crystalline ground quartz powder. For the seeding experiment, samples of both the fully amorphous and residual quartz powder were produced with 10 wt% cristobalite powder (Goresil; CE Minerals, Greeneville, TN) to act as a seed.

(2) Annealing

Samples were dry-pressed in a 25 mm die under an axial loading of 30 MPa. For the lower temperature, constant

L. Pinckney—contributing editor

Manuscript No. 33842. Received September 19, 2013; approved February 16, 2014.
*Member, The American Ceramic Society
**Fellow, The American Ceramic Society
†Author to whom correspondence should be addressed. e-mail: breneman@umich.edu

surface area study, the as-pressed pellets were annealed on an alumina plate for 0.5 to 24 h at 1200°C–1350°C in a box furnace under lab air with humidity ranging from 15%–60% relative humidity. Furnace ramp rates of 20°C/min on heating and 15°C/min on cooling were used. Note that these ramp rates place samples in the transformation range for 5–10 min, which is short compared to the annealing time. Temperatures reported are the furnace set point temperatures, and the furnace temperature readings have been verified by external thermocouple measurements to be accurate within ±7°C. The density of sintered samples were found by the Archimedes method, (ASTM C-373-88), to have 78%–86% full density and corresponding open porosity of 14%–22% with no closed porosity.

For the higher temperature study, in which concurrent densification was significant, the samples were briefly inserted and then removed from a furnace. These samples were lightly annealed at 1100°C to develop sufficient strength for handling but not form any cristobalite. The samples were then cut into bars of 3 mm thickness, 6 mm width, and length of 10–30 mm. These bars were suspended by a platinum wire in a furnace held at 1400C°–1650°C for 5 or 10 min. Densification of these samples varied significantly reaching nearly full density for samples sintered at 1550°C and above. As with the lower temperature samples, the porosities were found by the Archimedes method. The open porosity after 10 min at 1450°C was found to be 8%, after 5 min at 1550°C it was found to be 1.1%, and after 5 min at 1600°C it was found to be 0.5%.

Transformation kinetics were studied for samples annealed at 1200°C–1350°C with a 25°C step size between temperatures. The lower temperature limit of collected data in this study was chosen as a matter of practicality. At 1200°C, after a 30 h isothermal hold, samples were found to have a 0.23 ± 0.02 cristobalite fraction. The upper limit of 1350°C was found to be the highest temperature at which concurrent sintering during crystallization was not a concern. For all samples sintering occurred during the anneal. For samples annealed at 1350°C and below this sintering did not significantly impact the surface area of the powder. Samples sintered at 1400°C and above had significant densification which impacts the surface area of the material and the crystallization kinetics.

To obtain the isothermal transformation kinetics,[14] hold times at the reported temperature far exceeded time spent ramping to temperature or equilibrating at temperature. For samples annealed at 1350°C and below, the sample was inserted at room temperature and heated. Samples were exposed to temperatures in the transformation range for a short time relative to the isothermal hold. For samples annealed at 1400°C and above, the sample was inserted into the furnace at temperature. For these temperatures, based on sample dimensions and the thermal diffusivity of silica the estimated time for temperature to equilibrate is on the order of 10 s, which is short relative to the hold times of 5 and 10 min.

(3) Determination of Cristobalite Fraction

Following annealing, the fraction transformed was determined by means of quantitative powder X-ray diffraction (QXRD). As amorphous silica has no Bragg peak, we used 20 wt% TiO_2 anatase as an internal standard. Powder patterns were collected on a Rigaku Rotaflex (Rigaku Corporation, Tokyo, Japan) with CuK_α radiation operating at 40 kV and 100 mA (Rigaku Corporation). The scanning step size was 0.02° and scan speed 3 s per step. Scans were conducted from 18.5° to 28.5°. The (101) peak of cristobalite at 22° was compared to the (101) peak of the anatase at 25.3°, both being the primary diffraction peak of their compound.

To construct a standard, samples of pure cristobalite devitrified from the powder were mixed with untransformed starting material in known quantities. The pure cristobalite standard was produced by the method of Wang and Hon: 24 h anneal at 1550°C followed by grinding, a 12 h 1550°C anneal followed by grinding, and then a final 12 h 1550°C anneal.[5] These standards were mixed with 20 wt% anatase and measured by QXRD. The relative integrated intensities of the cristobalite and anatase signals were used to construct a calibration curve against which all samples were measured. The XRD scan to scan variation in measured cristobalite content of the same sample was found to be 1% between 20% and 80% cristobalite content and up to 5% for cristobalite contents outside this range.

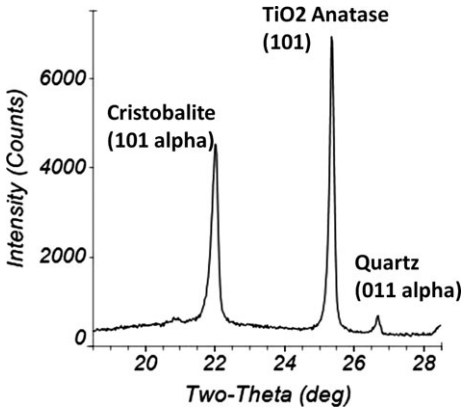

Fig. 1. Typical XRD Scan. Showing cristobalite, anatase, and quartz peaks. Cristobalite content found to be 21 ± 2% following a 45 min hold at 1325°C.

All samples were run in duplicate to minimize the effect of sample-to-sample variation. Two samples were simultaneously annealed and were separately ground and prepared for XRD. The cristobalite content produced from the XRD results was then averaged to produce the reported value. For simultaneously annealed samples, cristobalite content was found to vary by 0%–8%, with an average variation of 2%. The largest deviations were seen for cristobalite contents less than 20% or greater than 80%. For cristobalite content between 20% and 80%, the variation was found be ≤2%.

III. Results

(1) Transformation and Data Analysis

A typical XRD pattern can be seen in Fig. 1. For this example, the sample was annealed at 1325°C for 45 minutes and the cristobalite fraction was 0.21 ± 0.02. Note the anatase (101) standard peak at 25.3°, the cristobalite (101) peak rising from the amorphous background at 22°, and the residual quartz peak (011) at 26.7°. The quartz content was not quantified by a comparison to an established standard; however, it was observed in the raw powder to be compatible with the manufacturer's value of 5% by the standard established for cristobalite. Quartz content was observed to decrease from its initial value to that of background noise as samples exceeded 80% cristobalite content.

Figure 2 shows the complete dataset for the constant-porosity series as degree of transformation to cristobalite over the isothermal hold time at various temperatures. The lines seen in Fig. 2 are arbitrary and placed only to guide the eye. At 1500°C, 50% transformation to cristobalite was achieved in 10 min, whereas at 1200°C only 27% transformation was observed after 30 h.

For samples annealed from 1200°C to 1350°C, the degree of densification was minimal, and this transformation data were fit to an expression of the form of the Johnson–Mehl–Avrami–Kolmogorov equation:

$$Y = 1 - e^{-K(t)^n} \tag{1}$$

in which Y is fraction of cristobalite, t is time in minutes, K the kinetic constant, and n the time exponent.[14–16]

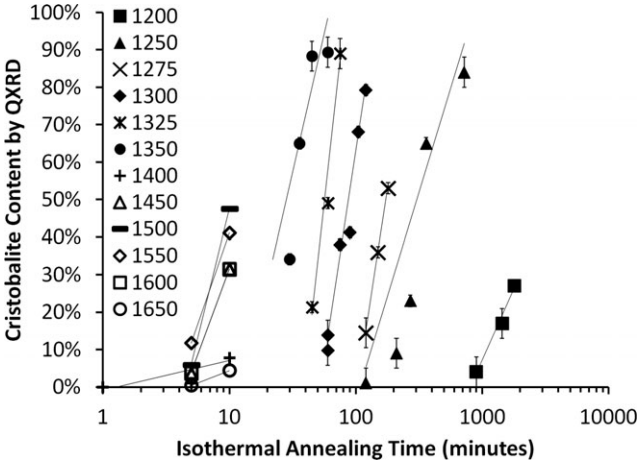

Fig. 2. Cristobalite content obtained by QXRD for varied annealing temperature (°C) versus isothermal hold time. (Linear fits plotted as visual guide only.).

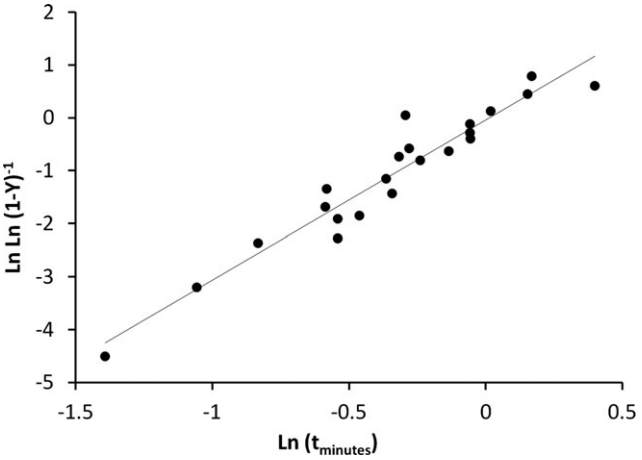

Fig. 4. Composite plot of the transformation data plotted as linearized form Eq. (1) Data from individual temperatures shifted on $\ln(t_{minute})$-axis. Data found to fit a single slope of with a time exponent $n = 3$.

The two unknowns, K and n, are extracted from the data. For each temperature, the averaged cristobalite content was used to plot the linearized form of Eq. (1): ln ln $[1/(1 - Y)]$ vs ln(t). This can be seen in Fig. 3. Plotted in this way the slope of a linear fit to the data provides the value for n, whereas the intercept provides the value of ln (K). The data at each temperature consisted of as few as three data points, which limits the accuracy with which slope can be determined. To account for this, a composite plot was produced by shifting the data from each temperature along the x axis by its x intercept, seen in Fig. 4. It was observed that this composite dataset fit a single slope with greater accuracy than the individual slopes found at each temperature. From this composite plot, it was found the data fit a single n value of $n = 3.0 \pm 0.6$ with error determined by residual sum of squares. Here, we are using the Avarami exponent as a fitting parameter and do not seek to interpret its values in terms of mechanism[16] or address crystallization at particle surfaces.[17,18]

Linear fits were then made for the data at each individual temperature using the n value determined from the composite plot, as seen in Fig. 3. The ln(K) values, seen below in Table I, were determined from the plots. Using these n and K values with Eq. (1), we calculated the time required to achieve cristobalite fraction of 0.1, 0.5, and 0.9 and plotted the results in the format of a TTT diagram in Fig. 5. This

Table I. JMAK Constants

$T \pm 7$°C	N	K	Ln K
1200	3.0 ± 0.6	0.00038	−7.9
1250	3.0 ± 0.6	0.0022	−6.1
1275	3.0 ± 0.6	0.0048	−5.3
1300	3.0 ± 0.6	0.0091	−4.7
1325	3.0 ± 0.6	0.015	−4.2
1350	3.0 ± 0.6	0.026	−3.7

constant porosity series represents the low-temperature leg of the TTT diagram, and appears to be linear.

For the transformation data in Fig. 5, the kinetic constant K can be expressed in Arrhenius form to find the apparent activation energy, Q for this low-temperature leg:

$$K = A\mathrm{e}^{(-Q/RT)} \tag{2}$$

where A is the preexponential term, R is the universal gas constant, and Q is the activation energy in J/mol. Recall that for a phase transformation, the activation energy involves the enthalpy of the transformation and the activation energies of the transport process. Figure 6 displays ln(K) vs $1/T$, which has a slope of Q/R. From Fig. 6, an apparent

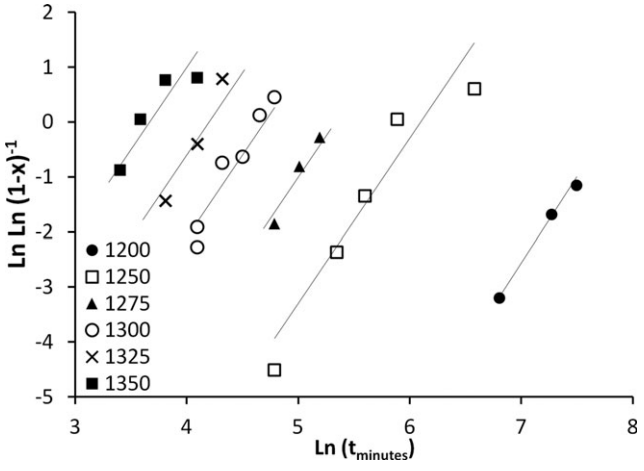

Fig. 3. Transformation data plotted in the form of the linearized Johnson–Mehl–Avrami–Kolmogorov equation, along with linear fits using a time exponent of $n = 3$.

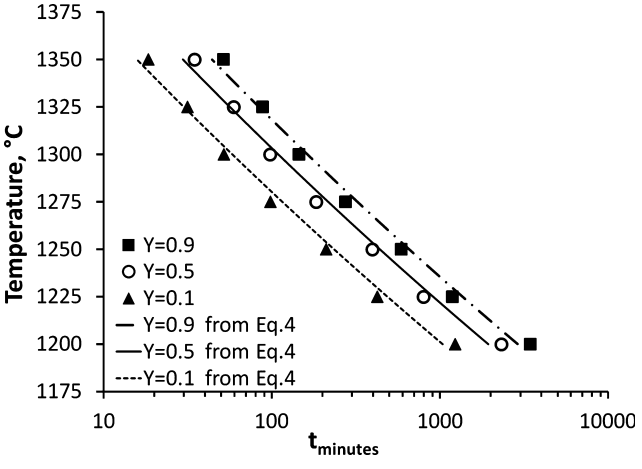

Fig. 5. Low-temperature leg of the Time–Temperature–Transformation (TTT) plot for Y 10%, Y 50%, and Y 90%. Individual points are interpolated using Eq. (1) from collected data at each temperature. Lines are plotted from Eq. (4).

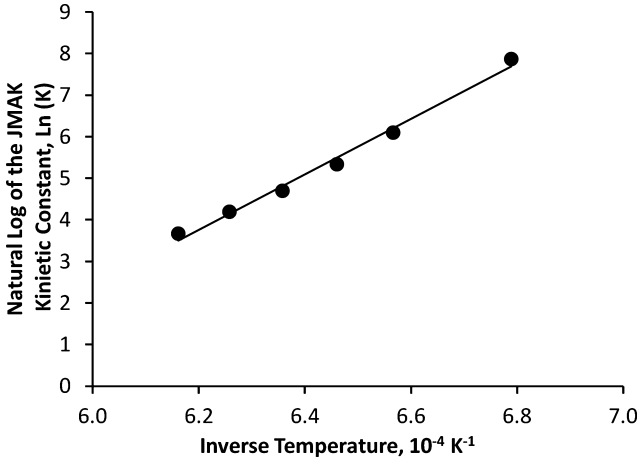

Fig. 6. Arrhenius plot of the kinetic constant K versus inverse temperature for the low-temperature leg of the TTT diagram.

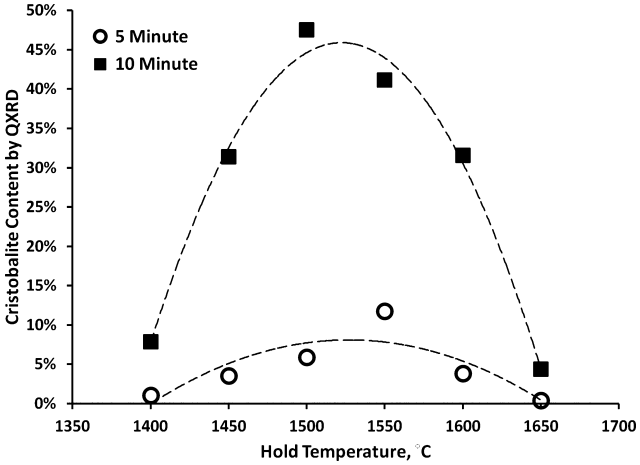

Fig. 7. Cristobalite content for brief annealing times at 1400°C–1650°C to approximate the temperature of maximum crystallization rate or "nose" of the TTT. (Dashed lines are for visual guide only.).

activation energy of 555 ± 24 kJ/mol is derived, where the uncertainty range is inferred from the residual sum of squares. The preexponential term A, inferred from regression of Fig. 6, is approximately $A = \exp(-36.7) = 4.7 \times 10^{-17}$. From this we can represent the kinetic constant that fits these data as follows:

$$K = (4.7 \times 10^{-17})\mathrm{e}^{-555\frac{\mathrm{kJ}}{\mathrm{mol}}/RT} \tag{3}$$

The low-temperature data can be described by

$$Y = 1 - \exp\left((4.7 \times 10^{-17})\mathrm{e}^{-555\frac{\mathrm{kJ}}{\mathrm{mol}}/RT}(t)^3\right) \tag{4}$$

This expression was used to calculate the lines seen in Fig. 5. This provides a good fit to the values calculated for each temperature observed in this study. The constants in Eq. (4) were determined from the data collected at all temperatures, and are, therefore, less sensitive to the observed experimental variation than the smaller individual temperature datasets.

The points in Fig. 5 for the Y_{10}, Y_{50}, and Y_{90} use the isothermal values from Eq. (4) to interpolate from the measured Y(t) values. Most of the directly measured data, as seen in Fig. 2, do not exactly fall at transformation fractions of 0.1, 0.5, or 0.9 cristobalite content. However, two measurements did come within experimental variation of 50% transformation allowing comparison to the Eq. (4) values. These two points, seen in Fig. 2, are 53 ± 2% after 180 min at 1275°C, and 49 ± 2% after 60 min at 1325°C. The 50% TTT line from Eq. (4) predicts t_{50} = 216 min at 1275°C, and 56 min at 1325°C.

This TTT diagram, Fig. 5, does not have the typical TTT "nose." This is because these temperatures fall far below the melting point of 1713°C; so the displayed range falls entirely in the low-temperature leg of the TTT curve. The location of the nose can be determined from the data at temperatures from 1450°C–1600°C. The direct observations in this range are plotted as degree of transformation by temperature in Fig. 7. The temperature of maximum crystallization rate falls between 1500°C and 1550°C. The specimens sintered rapidly at 1550°C and fully densified during the anneal. This would be expected to reduce crystallization rate as cristobalite is known to surface nucleate, so these higher temperature data for denser silica may not be directly comparable to the lower temperature data for porous silica. However, we have added the higher temperature direction observations falling near $Y = 0.1$ in Fig. 8, and they appear to agree with the lower temperature data. This allows us to estimate a more complete

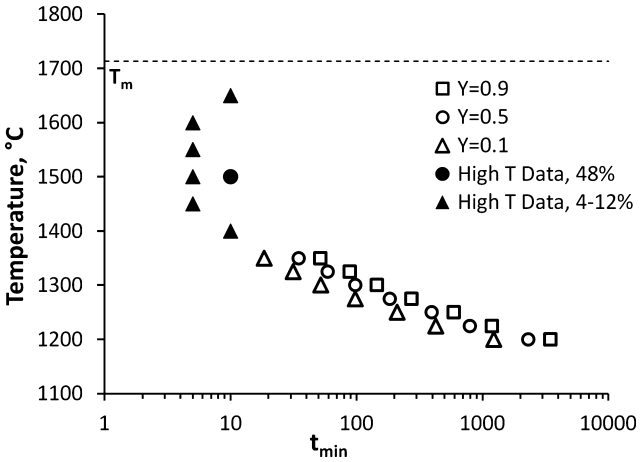

Fig. 8. Combination TTT plot of 10%, 50%, 90% transformation interpolated from Eq. (4) from 1200°C–1350°C and observations near 10% and 50% collected at high temperature.

TTT diagram including the nose around 1550°C and cristobalite melting temperature of 1713°C.[19]

(2) Seeding

Silica powder seeded with cristobalite was evaluated and compared with unseeded powder silica with and without residual quartz. A silica powder similar to the powder used in the previously discussed TTT study, but containing no residual quartz, was used as a comparison to evaluate the impact of the residual quartz on transformation. The effect of residual quartz content and cristobalite seeding was compared for: (1) a fully amorphous powder with no seed (2) a fully amorphous powder with 10 wt% cristobalite added (3) a powder with 5% residual quartz (4) a powder with 5% residual quartz with 10 wt% cristobalite added. Formulations are summarized in Table II.

A comparison of the cristobalite fraction after 1 h at various temperatures for the four powders can be seen in Fig. 9. For ease of comparison, a chart showing the temperature at which a given formulation achieved 0.5 cristobalite fraction after a 1 h hold is shown in Fig. 10. As expected, fully amorphous powder without cristobalite seed requires the highest temperature to transform in a 1 h anneal. It can be seen that the temperature at which the sample transforms after a 1 h hold is lowered in fully amorphous silica powder by the addition of cristobalite powder. This is also unsurprising, as it is expected that the crystalline powder will seed devitrification. The temperature at which the sample transforms after a 1 h

Table II. Formulations Used in Powder Comparison Study

Formulation	Fully amorphous powder (TECO-Sphere-A)	Residual quartz powder (TECO-Sphere-Microdust)	Cristobalite powder (Goresil)
1	100 wt%		
2	90 wt%		10 wt%
3		100 wt%	
4		90 wt%	10 wt%

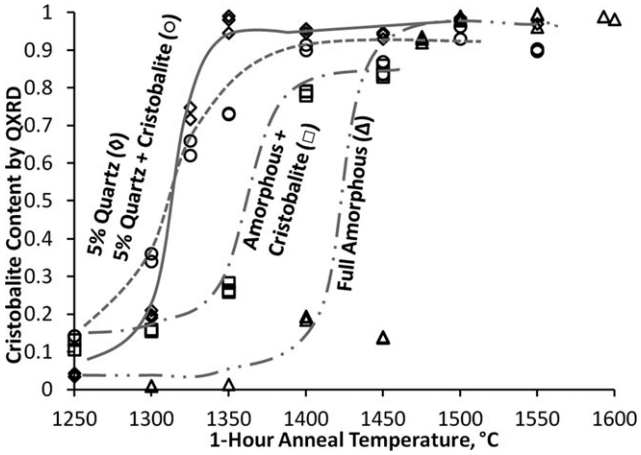

Fig. 9. Comparison of cristobalite content in varying powder formulations following 1-h isothermal annealing at various temperatures. Compares transformation of fully amorphous powder, fully amorphous powdered seeded with 10 wt% cristobalite, 5% residual quartz powder, and 5% residual quartz powder seeded with 10 wt% cristobalite.

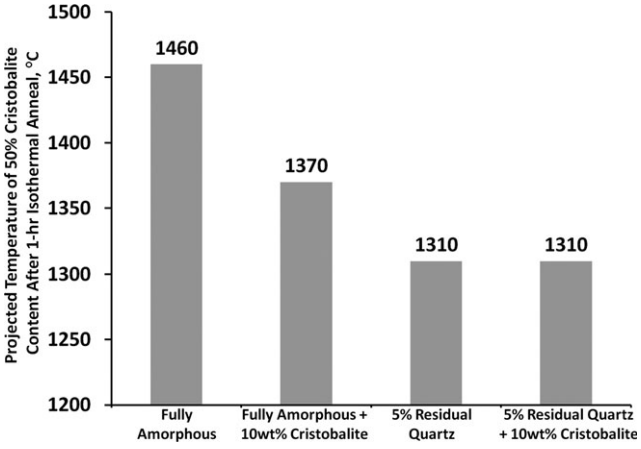

Fig. 10. Temperature for $t_{50\%}$ = 60 min

hold is even lower in the powder with residual quartz than in fully amorphous powder seeded with cristobalite. The residual quartz crystal has a larger impact on lowering the transformation temperature than seeding with cristobalite powder. For the mixed case, in which powder with residual quartz was seeded with cristobalite, the behavior was identical to unseeded powder. It should be noted that crystalline contents were measured by XRD and no confusion between quartz and cristobalite was possible. The quartz content was only observed to decrease, never increase, during devitrification to cristobalite.

(3) Microstructure of Cristobalite

Nucleation of cristobalite on the surface of the particles is suggested by the microstructure. Polished sections were prepared from epoxy-impregnated specimens polished to a 0.05 μm finish. Images were collected on FEI XL30 scanning electron microscope with a field-emission gun electron source (Hillsboro, OR).

Figures 11(a–d) shows backscattered electron imaging of samples with 11%, 25%, 55%, and 84% cristobalite. These samples fall in the 1200°C–1350°C range of minimal densification with relatively constant surface area. Using electron backscatter imaging, the small density difference between the amorphous and crystalline state provides contrast, in that the cristobalite is slightly darker. The presence of a cristobalite layer can also be inferred from the pattern of microcracks in the surface layer of the larger particles. This cracking occurs during the transformation from the high-temperature β-cristobalite phase to the low-temperature α-cristobalite phase upon cooling below 250°C.[20] In a partially crystalline particle, stress will develop when the volume change associated with the β-α transformation is constrained by the static amorphous region. As seen in Fig. 11 over the course of transformation, cristobalite forms a shell layer around the still amorphous core. This is the expected behavior as it is widely known that cristobalite preferentially nucleates at the surface.[3,8,21] This being a powder sample, cristobalite has apparently nucleated at the internal free surfaces and progressed inward from the particle surface leaving an amorphous core. The microcracks pass through the cristobalite shell region and terminate at the amorphous–crystalline interface.

Figure 12 shows a sample with 41% cristobalite sintered at 1550°C which sintered to high density after only a 10 min anneal. Cracked particles of the same 5–50 μm scale, similar to the larger spheres from the powder, can be seen embedded in a matrix. The area fraction of these embedded fractured particles matches that of the fraction cristobalite observed by XRD.

IV. Discussion

(1) Comparison to Prior Work

The transformation behavior observed in this study can be compared to various published results, seen in Fig. 13. The published kinetic data these studies in several silica systems were used to plot $Y = 0.5$ values in the format of a TTT diagram. The direct observation of $Y = 0.48$ observed after 10 min at 1500°C is plotted as well. The wide range of the transformation behavior is immediately apparent. High-purity silica transforms at the highest temperatures over the longest times.[6] Less pure refractory grade commercial silica powder, comparable in purity to the powder used in this study, transforms over shorter times and can be accelerated by seeding with cristobalite to transform even more quickly.[5] The powder used in this study can be seen to transform at even shorter times. This corroborates the findings of the powder comparison study in which purely amorphous silica seeded with cristobalite had slower transformation than silica with residual quartz. Doped silica systems such as borosilicate glass and NaO_2-doped silica are found to transform at lower times and temperatures.[4,22] Among the studies of nominally pure SiO_2 systems we then see a progression, where the slowest kinetics belong to the purest material. Overall, we observed that lower purity accelerates the transformation, cristobalite seeding accelerates the transformation further, and indicated in this study, residual quartz crystallinity accelerates the transformation still further. We see the powder with residual quartz possesses the fastest transformation kinetics of nominal pure SiO_2 systems, but is slower than doped silica based systems.

(2) Concurrent Densification and the Temperature of Maximum Transformation Rate

The apparent "nose" of the TTT diagram, or the temperature of maximum transformation rate, was observed to fall

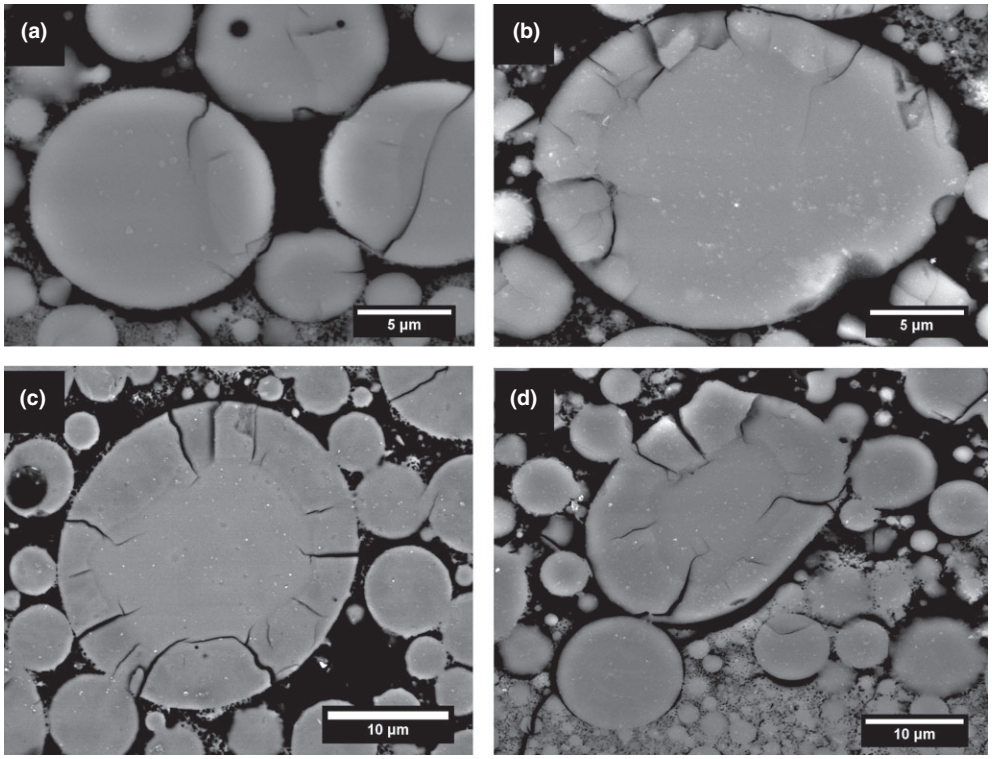

Fig. 11. Partially crystalline material imaged with backscattered electrons. The growth of the cristobalite crystalline phase on particle surface and the development of a core–shell morphology is visible. (a) 11% cristobalite content. (b) 25% cristobalite content. (c) 55% cristobalite content. (d) 84% cristobalite content.

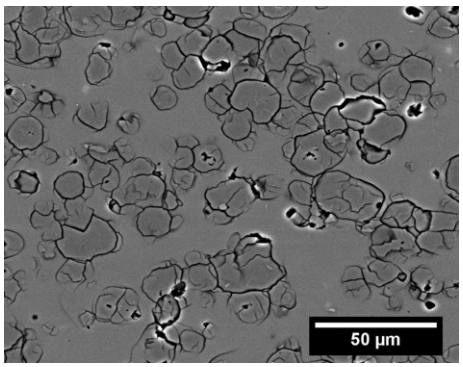

Fig. 12. Sample annealed at 1550°C for 10 min imaged by backscattered electrons, where cristobalite is slightly darker in contrast. This specimen had 41% cristobalite by QXRD. Cracking is from the transformation to alpha-cristobalite on cooling.

between 1500°C and 1550°C. However, the kinetics of crystallization at the observed nose are complicated by concurrent sintering densification during crystallization. Concurrent crystallization and sintering can be a complex phenomena common in glassy powders, which has been previously reported on by Prado *et al.*[12,13] In this study, it was observed that the samples annealed above 1400°C densified to a far greater extent than those annealed at lower temperatures. In a surface nucleating crystallization process such as the current study this can potentially have a large impact on the kinetics of the reaction by reducing the number of nucleation sites available. In particular, at temperatures of 1550°C and above the samples were observed to densify into a dense glass with closed porosity. It is unclear from this study whether this densification impacted the apparent transformation rate. It is possible that at temperatures at which sintering densification occurs rapidly the kinetics are slowed due to a reduction in the available number of nucleation sites as the surface area decreases.

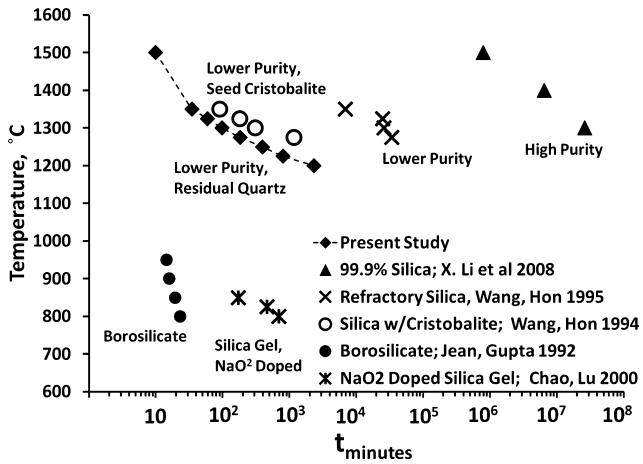

Fig. 13. Comparison of results to published data for crystallization of silica to cristobalite presented in TTT format for $Y = 0.5$. Results from this study include the additional direct observation of $Y = 0.48$ for 10 min anneal at 1500°C.

(3) Seeding and Residual Quartz Effect

lAs illustrated in Figs. 9 and 10, the temperature at which a sample crystallized in a 1 h anneal was lowered by seeding with cristobalite, but lowered more by use of a powder with residual quartz. The effect is prominent when one looks at the temperature at which the material passes the 50% cristobalite conversion mark in a 1 h anneal. Seeding with cristobalite has a dramatic effect, lowering the temperature to pass 50% conversion by 90°C. However, powder with residual quartz shows an even more dramatic decrease of 150°C for 50% conversion in a 1 h anneal. Further, in material with residual quartz crystallinity, the addition of cristobalite powder had no effect on transformation. This behavior is unexpected. The apparent conclusion is that, paradoxically, residual quartz is more effective at accelerating the formation of cristobalite than the

addition of cristobalite seed powder. In addition, the effect of the residual quartz is such that the further addition of cristobalite powder has no observed effect.

It is surprising to find quartz accelerating the transformation to cristobalite to a greater degree than cristobalite. However, the details of the system must be remembered. Seed cristobalite is crystalline powder mechanically mixed with amorphous silica powder. One expects cristobalite-silica contact to be very limited in such a system. On the other hand, residual quartz is presumably retained within the silica particles as an unmelted fraction from the drop-furnace process. This presents the possibility that the observed behavior arises from differences in the distribution of the cristobalite seed and residual quartz rather than the relative potency of quartz and cristobalite in accelerating crystallization. A study comparing powders incompletely amorphized from cristobalite starting material may shed more light on this behavior. It is not known by what mechanism residual quartz crystal accelerates the formation of cristobalite, but given the significant effect further study is warranted.

V. Conclusions

The degree of transformation (Y) of sintered silica glass powder to cristobalite, annealed at 1200°C–1350°C under conditions where the porosity was constant, can be represented by an expression of the form: $Y = 1 - \exp((4.7 \times 10^{-17})e^{-555\frac{kJ}{mol}/RT}(t)^3)$. Short anneals at 1400°C–1650°C showed that the temperature of maximum transformation rate was between 1500°C and 1550°C. At these higher temperatures, the powder densified by sintering, but the transformation kinetics agreed with the lower temperature kinetics extrapolated to 1400°C

Seeding of fully amorphous silica powders with cristobalite powder lowers the temperature required to transform the material. Residual quartz from incompletely amorphized silica also lowers the transformation temperature to a larger extent than cristobalite seeding.

Acknowledgments

This research was supported by the Defense Advance Research Projects Agency (DARPA) under grant HR001-08-1-0075, Principal Investigator Suman Das, Georgia Institute of Technology, Program Officer W.S. Coblenz and the Office of Naval Research, Scientific Officer David Shifler. The authors thank the Georgia Tech team and PCC Airfoils for assistance. We thank Professor Martha Mecartney, University of California-Irvine, and Dr. John Mansfield, University of Michigan, for assistance with microscopy and microstructure characterization.

References

[1]N. G. Ainslie, C. R. Morelock, and D. Turnbull, "Devitrification Kinetics of Fused Silica"; pp. 97–109 in *Symposium on Nucleation and Crystallization in Glasses and Melt*, Edited by M. K. Reser. American Ceramic Society, Columbus, OH, 1966

[2]F. E. Wagstaff and K. J. Richards, "Preparation and Crystallization Behavior of Oxygen-Deficient Vitreous Silica," *J. Am. Ceram. Soc.*, **48** [7] 382–3 (1965).

[3]A. G. Verduch, "Kinetics of Cristobalite Formation from Silicic Acid," *J. Am. Ceram. Soc.*, **41** [11] 427–32 (1958).

[4]C. H. Chao and H. Y. Lu, "Crystallization of Na_2O-Doped Colloidal Gel-Derived Silica," *Mater. Sci. Eng. A-Struct. Mater. Prop. Microstruct. Process*, **282** [1–2] 123–30 (2000).

[5]L. Y. Wang and M. H. Hon, "The Effect of Cristobalite Seed on the Crystallization of Fused-Silica Based Ceramic Core - a Kinetic-Study," *Ceram. Int.*, **21** [3] 187–93 (1995).

[6]X. M. Li, X. W. Yin, L. T. Zhang, and S. S. He, "The Devitrification Kinetics of Silica Powder Heat-Treated in Different Conditions," *J. Non-Cryst. Solids*, **354** [28] 3254–9 (2008).

[7]A. Kazemi, M. A. Faghihi-Sani, and H. R. Alizadeh, "Investigation on Cristobalite Crystallization in Silica-Based Ceramic Cores for Investment Casting," *J. Eur. Ceram. Soc.*, **33** [15–16] 3397–402 (2013).

[8]F. E. Wagstaff and K. J. Richards, "Kinetics of Crystallization of Stoichiometric SiO_2 Glass in H_2O Atmospheres," *J. Am. Ceram. Soc.*, **49** [3] 118–21 (1966).

[9]T. Honma, N. Tamura, K. Saito, and E. Sekiya, "Difference in Structural Relaxation Times of Inner Surface and Inner Bulk Region of Silica Glass Arc Tube," *New J. Glass Ceram.*, **3**, 48–52 (2013).

[10]E. Opila, "Influence of Alumina Reaction Tube Impurities on the Oxidation of Chemically-Vapor-Deposited Silicon-Carbide," *J. Am. Ceram. Soc.*, **78** [4] 1107–10 (1995).

[11]P. P. Bihuniak, "Effect of Trace Impurities on Devitrification of Vitreous Silica," *J. Am. Ceram. Soc.*, **66** [10] C188–9 (1983).

[12]M. O. Prado, M. L. F. Nascimento, and E. D. Zanotto, "On the Sinterability of Crystallizing Glass Powders," *J. Non-Cryst. Solids*, **354** [40–41] 4589–97 (2008).

[13]M. O. Prado and E. D. Zanotto, "Glass Sintering with Concurrent Crystallization," *C. R. Chim.*, **5** [11] 773–86 (2002).

[14]M. Avrami, "Kinetics of Phase Change I-General Theory," *J. Chem. Phys.*, **7** [12] 1103–12 (1939).

[15]W. A. Johnson and R. F. Mehl, "Reaction Kinetics in Processes of Nucleation and Growth," *Trans. Am. Inst. Min. Metall. Eng.*, **135**, 416–42 (1939).

[16]M. C. Weinberg, D. P. Birnie, and V. A. Shneidman, "Crystallization Kinetics and the JMAK Equation," *J. Non-Cryst. Solids*, **219**, 89–99 (1997).

[17]I. Gutzow, R. Pascova, A. Karamanov, and J. Schmelzer, "The Kinetics of Surface Induced Sinter Crystallization and the Formation of Glass-Ceramic Materials," *J. Mater. Sci.*, **33** [21] 5265–73 (1998).

[18]A. Karamanov, I. Avramov, L. Arrizza, R. Pascova, and I. Gutzow, "Variation of Avrami Parameter During Non-Isothermal Surface Crystallization of Glass Powders with Different Sizes," *J. Non-Cryst. Solids*, **358** [12–13] 1486–90 (2012).

[19]W. A. Deer, R. A. Howie, and J. Zussman, *An Introduction to the Rock Forming Minerals*. Prentice Hall, Essex, UK, 1966.

[20]D. R. Peacor, "High-Temperature Single-Crystal Study of Cristobalite Inversion," *Z. Kristall*, **138**, 274–98 (1973).

[21]F. E. Wagstaff, "Crystallization Kinetics of Internally Nucleated Vitreous Silica," *J. Am. Ceram. Soc.*, **51** [8] 449–52 (1968).

[22]J. H. Jean and T. K. Gupta, "Crystallization Kinetics of Binary Borosilicate Glass Composite," *J. Mater. Res.*, **7** [11] 3103–11 (1992). □